PROCEEDINGS OF SPIE

SPIEDigitalLibrary.org/conference-proceedings-of-spie

Numerical integration of slope data with application to deflectometry

Ramirez-Andrade, Ana, Porras-Aguilar, Rosario, Falaggis, Konstantinos

Ana H. Ramirez-Andrade, Rosario Porras-Aguilar, Konstantinos Falaggis, "Numerical integration of slope data with application to deflectometry," Proc. SPIE 11490, Interferometry XX, 1149009 (21 August 2020); doi: 10.1117/12.2570600



Event: SPIE Optical Engineering + Applications, 2020, Online Only

Numerical integration of slope data with application to deflectometry

Ana H. Ramirez-Andrade*a, Rosario Porras-Aguilara, Konstantinos Falaggisb,

^aOptical Science and Engineering Department, University of North Carolina at Charlotte, 9201
University City Blvd., Charlotte, North Carolina 28223, USA;

^bMechanical Engineering and Engineering Science Department, University of North Carolina at Charlotte, 9201 University City Blvd., Charlotte, North Carolina 28223, USA

*correspondence author: aramir28@uncc.edu

ABSTRACT

This work presents a stable noise-robust numerical integration technique derived from a gradient representation of the Q-Forbes polynomials for surfaces with axial symmetry. This modal-integration technique uses an orthogonalization process through the Householder reflections to obtain a numerically orthogonal set for the surface slopes that is used to reconstruct the surface shape. It is shown that for typical Deflectometry measurements, the resulting random component of the uncertainty after numerical integration has a root mean square error well below 1nm.

Keywords: Optical metrology, modal reconstruction Q Forbes polynomials, Deflectometry.

1. INTRODUCTION

High-precision metrology of three-dimensional shape measurements has become a key technology in industrial applications, including the fabrication of optical surfaces. Phase Measuring Deflectometry (PMD) invented in 1999 by Häusler[1]–[3] measures the slope of specular samples. Deflectometry is an optical shape measurement technique to measure micro-size to large specular surfaces, including aspheric mirrors, freeform optics, dynamic specular surfaces, and in-line measurements in ultra-precision manufacturing environments [3]. PMD has high repeatability; it routinely achieves nanometer-level accuracy for local surface defects. However, PMD does not provide direct shape measurements. The measured slope needs to be integrated, which results in errors in the reconstructed form. These errors may be small for smaller objects but increase significantly with the size of the sample.

In this work, we propose a modal integration technique to reconstruct the shape of the sample. This is achieved by deriving an orthogonal set of gradients that correspond to modes based on Q Forbes polynomials. The slope data can directly be fitted to the gradients, and the corresponding coefficients can be translated to the individual Q Forbes mode coefficients.

This work is organized as follows: Section 2 describes the principles of Deflectometry. Section 3 reviews the Q Forbes polynomials that define an optical surface using the best-fit sphere and departure term constructed as a linear combination of the basis formed by these polynomials. Section 4 describes our proposed modal integration using Q polynomials and the results when applying the proposed integration method for the case of an Asphere. The stability of this numerical integration technique in the presence of noise is analyzed. The discussions are presented in Section 5.

2. BASIC PRINCIPLES OF DEFLECTOMETRY

The PMD metrology hardware is relatively simple; it consists of a display, a camera, and the sample under test, as shown in Fig. 1. A pattern is displayed on a screen, and the camera captures the reflection from the sample. The deformations in the captured fringe patterns are related to the slope of the sample. The quest is to obtain the surface of the sample under test using the measured slope. In well-calibrated camera systems, a ray is traced back from the camera to the sample (see Fig. 1 blue line), and after reflection back to the corresponding pixel in the display (see Fig. 1, black line). The location of the pixel in the display can be estimated with sub-fringe resolution using sinusoidal fringe-patterns with phase-shifting-techniques[4]. Both horizontal and vertical sinusoidal fringe patterns are necessary to recover the corresponding position in x- and y-direction. The location of the display pixel can directly be converted to the slope of the sample using:

Interferometry XX, edited by Michael B. North Morris, Katherine Creath, Rosario Porras-Aguilar, Proc. of SPIE Vol. 11490, 1149009 © 2020 SPIE ⋅ CCC code: 0277-786X/20/\$21 ⋅ doi: 10.1117/12.2570600

$$\Delta x = d \tan 2\alpha \,, \tag{1}$$

where d is the distance between the screen and the object, and Δx is the position of the pixel relative to the reference point. The classical trigonometric identities reveal that the slope can only be calculated correctly if the distance d between screen and sample is known. As shown in Fig. 2, there are multiple possibilities for height and slope combinations for a given pair of camera ray and display pixel. This problem is the so-called height-slope ambiguity [5] and is solved using regularization techniques. Once this is overcome, the system can measure very high surface slopes with high spatial resolution.

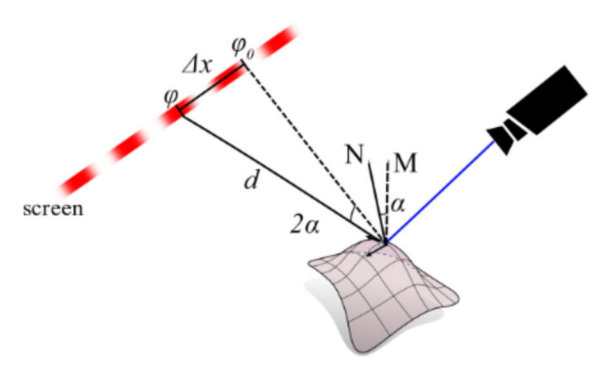


Figure 1. Measuring principle of deflectometry. Single ray is reflected from the surface into the camera. An angle change of the surface under test with respect to a reference orientation introduces a double angle 2α to the reflected ray.

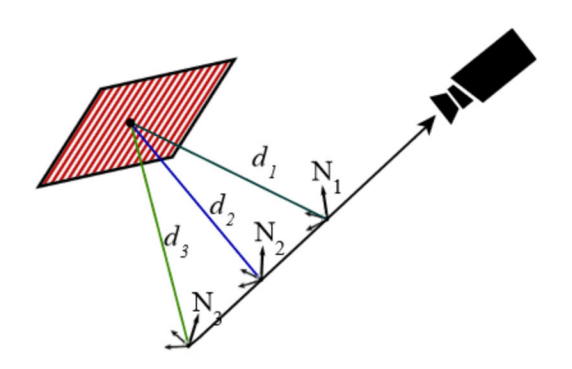


Figure 2. Deflectometry inherent height-slope ambiguity. For every value of the recovered phase of the reflected sinusoidal patterns in each camera pixel, there are multiple height/slope combinations.

2.1 Height-slope ambiguity

Regularization can be provided in different forms. In monoscopic deflectometry (single camera, single screen) assumptions can be made if the surface is very similar to the pre-known shape [6]. An alternative is stereo deflectometry [5], where adding a second camera enables measuring the surface normal for each point of the object. Another method records patterns from multiple screens to create enough redundant data for each camera pixel to overcome the height-slope ambiguity. A similar effect is obtained when shifting the display laterally [7] – in some applications, the reconstruction is simplified using telecentric camera systems with multiple screens [8]. Other techniques use a sensor to measure the distance to a single point on the surface under test [9]. Once the height-slope ambiguity problem is solved, PMD systems routinely measure slopes with μrad precision [5], and the system in [10] reported an uncertainty down to 100nrad.

This slope data can also be converted into a curvature map [5] that is particularly useful to measure local surface features [11] with nanometer precision. However, PMD has its challenges. The numerical integration is prone to calibration and other systematic errors that lead to significant shape deviations (higher than 500nm), especially for large samples [12]. It

is, therefore, important to distinguish between local and global errors. The local error is mainly caused by camera noise [13].

2.2 Numerical integration in deflectometry

As mentioned before, in order to obtain the 3D shape of the specular sample, a two-dimensional integration procedure that uses the measured slopes is necessary. Commonly, there are two major families of numerical integration techniques. The so-called (deterministic) modal methods and the so-called zonal methods. The zonal reconstruction uses local relations between heights and slopes to obtain the final height estimate using a least-square approach. A vast number of authors have investigated zonal methods, ranging from the development of Southwell algorithms in the late 1970s [14] to more recent methods specifically designed for PMD [15], [16]. The latter were investigated in order to accurately estimate the height values by matching their calculated first derivatives with the measured slopes in the least-squares sense.

In modal reconstruction, the surface shape and its corresponding slope are described using a specific analytical model that allows relating the measured slope to the mode coefficients that, when superimposed, form the height distribution. Examples are many, as, e.g., orthogonal polynomials Zernike [17], [18] Chebyshev [19], Legendre [20], B-spline [21], or sinusoidal curves [22]. More recently, modal integration was proposed as part of a global optimization process [23] to reduce the reprojection error when performing the ray-tracing procedure, where Chebyshev, Zernike, or B-spline polynomials have been employed in reference [23].

Modal methods are commonly used in optical design and fabrication to mathematically describe the surface. In this regard, Zernike polynomials have been widely used due to their orthogonality and balanced representation of classical aberrations yielding minimum variance over a circular pupil. They have been first employed by F. Zernike, in his phase-contrast method for testing circular mirrors [24]. Another interesting development is the Q Forbes polynomials [25] that started a decade ago and gained increased relevance due to its properties related to optical fabrication since these polynomials facilitate the enforcement of manufacturability constraints during the design of optical elements, such as rotationally symmetric aspheres and freeform optics [25]–[30].

3. FORBES QBFS POLYNOMIALS

Greg Forbes developed a new set of orthogonal polynomials over a circular aperture. This set is referred to as Q_{bfs} and orthogonalized to the mean square gradient over an enclosing circular aperture to facilitate measures of manufacturability [25]. Commonly, it is desired to express an optical surface using the departure of the surface from its best-fit sphere (or best-fit conic) with an orthogonal set of polynomials. Motivated by that, Forbes decided to define so-called Q-polynomials with orthogonal gradients to enable estimates for manufacturability of these surfaces and the integration with optical design environments. Orthogonal polynomials have the advantage of expressing an optical surface as a spectrum of coefficients in decreasing order, which helps in interpreting the frequency content of an optical surface. In terms of optical manufacturing and testing of an optical surface, the polynomial shapes with minimal Sag (e.g., with respect to a sphere) are easier to be produced. Thus, the rate of change of departure of a surface along the local normal from its best-fit sphere must be specified, because the local principal curvatures are related to the derivatives of the departure. In this context, the Sag $z(\rho,\theta)$ in polar coordinates of an optical element can be written as in reference [25]:

$$z(\rho,\theta) = \frac{c_{bfs}\rho^2}{\left(1 + \sqrt{1 - c_{bfs}\rho^2}\right)} + D_{bfs}\left(\frac{\rho}{\rho_{max}}\right),\tag{2}$$

where c_{bfs} is the curvature of the best-fit sphere, ρ_{max} is the aperture radius, and the second term,

$$D_{bfs}(u) = \frac{u^2(1-u^2)}{\sqrt{1-c_{bfs}\rho_{max}^2 u^2}} \sum_{m=0}^{M} a_m Q_m^{bfs}(u^2),$$
 (3)

describes the departure from the best-fit sphere, where a_m is the mode coefficient of the mode Q_m^{bfs} , M is the total number of modes used, and u is the normalized radial coordinate to the aperture. Every mode Q_m^{bfs} is calculated using the recurrence formula

$$Q_m^{bfs}(x) = \frac{1}{f_m} \left[P_m(x) - g_{m-1} Q_{m-1}^{bfs}(x) - h_{m-2} Q_{m-2}^{bfs}(x) \right]. \tag{4}$$

The recurrence variables g_m , h_{m-1} , and f_{m+1} are found iteratively with initial values m=2, $f_0=2$, $f_1=\sqrt{19}/2$, and $g_0=-0.5$, and using the equations:

$$h_{m-2} = -\frac{m(m-1)}{2f_{m-2}},\tag{5}$$

$$g_{m-1} = -\frac{(1 + g_{m-2}h_{m-2})}{f_{m-1}},\tag{6}$$

$$f_m = \sqrt{(m(m+1) + 3 - g_{m-1}^2 - h_{m-2}^2)}$$
 (7)

and the auxiliary polynomials, $P_m(x)$ are a special form of Jacobi polynomials that satisfy a three-term recurrence:

$$P_m(x) = (2 - 4x)P_{m-1}(x) - P_{m-2}(x), \tag{8}$$

where the first two auxiliary polynomials are $P_0(x) = 2$, and $P_1(x) = 6 - 8x$, respectively. The first three modes of the polynomial set Q_m^{bfs} are given by [25]:

$$Q_0^{bfs}(x) = 1, \qquad Q_1^{bfs}(x) = \frac{1}{\sqrt{19}}(13 - 16x), \qquad Q_2^{bfs}(x) = \sqrt{\frac{2}{95}}[29 - 4x(25 - 19x)].$$
 (9)

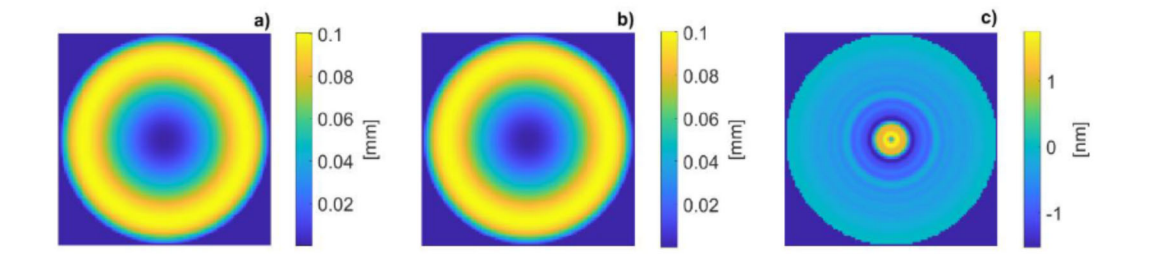


Figure 3. Result of the modal integration. a) Original surface with sag $100\mu m$. b) Recovered surface from modal integration. c) Residual of the recovered surface, with RMSE = 0.57122 nm and PV = 3.649 nm.

4. PROPOSED EXTENSION OF Q FORBES POLYNOMIALS FOR SLOPE FITTING WITH APPLICATIONS TO DEFLECTOMETRY

The analytical expression of the slope in x- and y-direction of the departure from the best-fit sphere in Eq. (3) can be easily written after Eqs. (4) and (8) using the chain rule. The resulting expression for both derivatives can also be expressed as a three-term recurrence relation. It is important to notice that besides the linear superposition of the basis of the vector space defined by every $Q_m^{bfs}(x)$ we also need to calculate the derivative of the first factor in Eq. (3). The new basis generated after the derivatives of the $D_{bfs}(u)$ have lost the orthogonality properties of the original polynomial basis Q_{bfs} due to the multiplicative factor in Eq. (3). This translates into the need to use an orthogonalization process that constructs a new basis to perform the modal reconstruction. In practice, the Gram-Schmidt procedure can lead to ill-posed Q matrices, and hence,

this work implemented a QR Decomposition using Householder reflections[31]. Consider the measured gradient of $D_{bfs}(u)$ as function of the orthogonal components (HR_x, HR_y) found from the Householder reflections:

$$\left(S_{x}, S_{y}\right) = \sum_{n=0}^{N} b_{n} \left(HR_{x}, HR_{y}\right),\tag{10}$$

where S_i (i = x, y) is the component in the *i*-direction of the measured gradient, b_n is the weighting coefficient for each gradient mode. The derivatives in Eq. (10) can also be calculated from the definition of the departure term in Eq. (3):

$$(S_x, S_y) = \vec{\nabla} \left[\frac{u^2 (1 - u^2)}{\sqrt{1 - c_{bfs} \rho_{max}^2 u^2}} \sum_{n=0}^{N} a_n Q_n^{bfs} (u^2) \right]. \tag{11}$$

Finally, the coefficients a_n can be found from the obtained b_n coefficients as:

$$D_{bfs}(u) = \sum_{n=0}^{N} a_n f \times Q_n^{bfs}(u^2),$$
 (12)

where $f = u^2(1 - u^2)/\sqrt{1 - c_{bfs}\rho_{max}^2 u^2}$ is the first factor in the square brackets in Eq. (11).

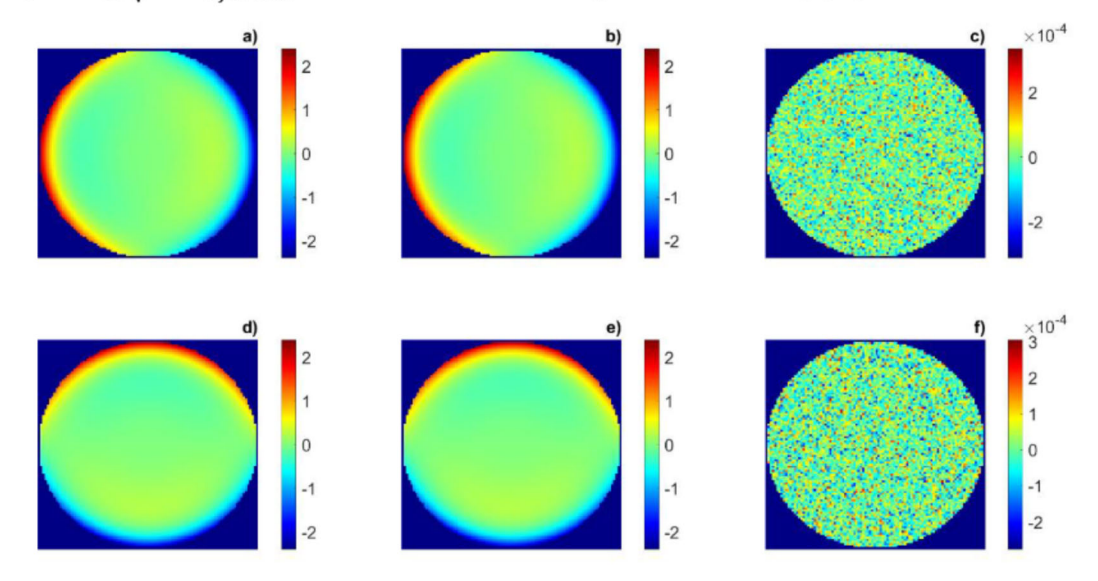
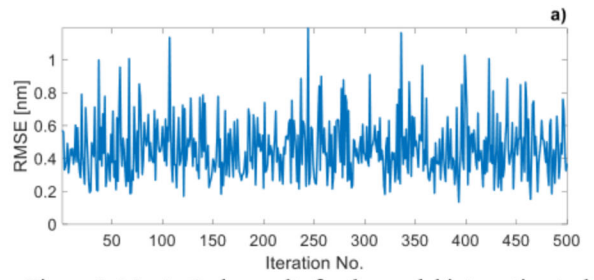


Figure 4. Results of the modal integration in the slope. a) Original x-direction gradient component. b) Recovered x-direction gradient component, RMSE = 7.9658e-05. d) Original y-direction gradient component. e) Recovered y-direction gradient component. f) Residual of the recovered x-direction gradient component, RMSE = 7.99013e-05. The residuals show the initial local error in the slope $\epsilon = 80\mu$ rad.

In order to test the modal integration using the best-fit sphere Q polynomial, we use the specifications of the Asphere surface presented in [27]. This optical element is fitting to the best-fit sphere with a radius equal to 22.2378 mm, while the departure from the sphere is defined by the first six modes with the coefficients: 471316, -90550, 16631, -3810, 478, and -113 nm over a circular aperture of 20 mm radius. The original surface for the part in Fig. 3 has a 100µm Aspheric departure. The x- and y-components of the corresponding slope is shown in Fig. 4a and 4d, respectively. The (simulated) measured slopes with a PMD typical level of noise, is shown in Fig. 4b and 4e, and the corresponding errors is shown in Fig. 4c and 4f. The set of orthogonal gradients have been fitted to the x- and y- components of the slope of the Q Forbes polynomial. In a subsequent step, the fitted coefficients have been used to reconstruct the shape, as shown in Fig. 3. The results show that the random error component in the slope measurements results in surface uncertainty levels in the nanometric scale. Notably, the

root mean square error (RMSE) of the modal technique is less than 1nm. A Monte Carlo simulation has also been used to evaluate the performance of the modal integration further; a slope uncertainty equal to 80μ rad was used in 500 iterations to assert the confidence of the results. Fig. 5.a) shows that the RMSE fluctuations are, for most cases, near 0.5 nm, but mostly below 1nm. The peak to valley (PV) error is found mostly near \sim 4 nm, but always well below 10nm.



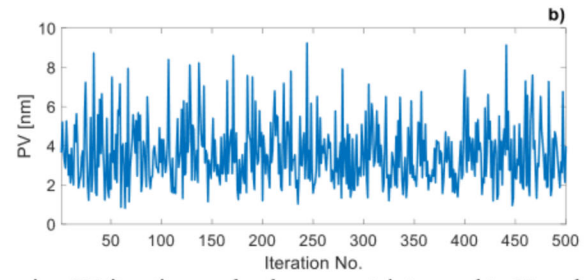
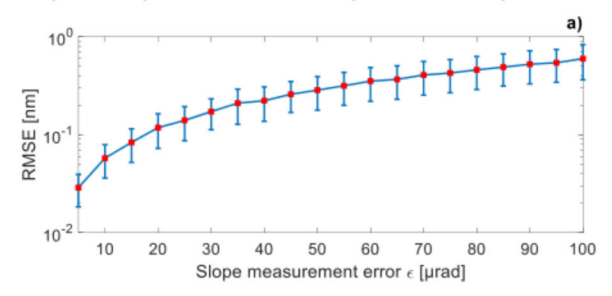


Figure 5. Monte Carlo results for the modal integration technique using 500 iterations and a slope uncertainty equal to 80μrad a) RMSE (mean value 0.461 nm) and PV error (mean value 3.597 nm).



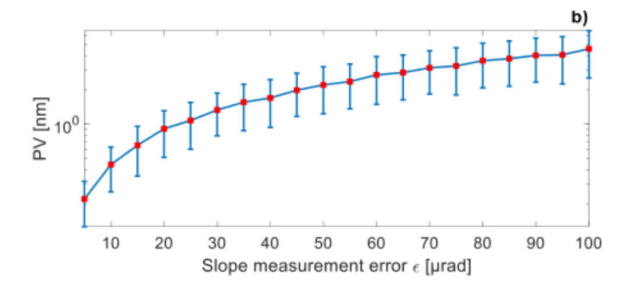


Figure 6. Quantification of the measurement error of the proposed numerical integration technique using the gradient data with a slope measurement error ϵ between 5 and 100 μ rad (500 Monte-Carlo iterations each). The PV and RMSE confidence intervals are plotted for each a) RMSE and b) PV error

A second Monte Carlo simulation was performed to examine the reconstruction uncertainty for different values of the slope error in the interval from 5 to 100 µrad. Fig. 6 shows that the uncertainty of the modal integration is as 0.028825nm in the RMSE and 0.59601 nm for the PV error for the case of 5µrad error in the measured slope, an as large as 0.22097nm and 4.5832nm for the RMSE and PV error, respectively, if the slope error is 100 µrad. These results show that even for cases where the recovered slope from a typical PMD system sensor setup is subject to random errors, it is still possible to obtain stable numerical integration results in the nanometer level uncertainty.

5. CONCLUSIONS

Q Forbes polynomials have been traditionally used to describe the Sag departure of surfaces to meet the needs of the optical fabrication and design. In this work, we have extended the use of these polynomials for numerical integration in order to recover surface shapes from slope data via modal integration with gradient representations of Q Forbes polynomials. We show that the modal integration technique is robust to noise for a wide range of noise levels that are typically encountered in PMD measurements. Even for higher levels of noise, the resulting random error component of the reconstructed shape is in the order of tenths of nm.

REFERENCES

- [1] G. Häusler, C. Faber, E. Olesch, S. Ettl, and B. Staudtstr, "Deflectometry vs . Interferometry," vol. 8788, no. 0, pp. 13–16, 2013.
- [2] C. Faber, E. Olesch, R. Krobot, and G. Häusler, "Deflectometry challenges interferometry: the competition gets tougher!," 2012, p. 84930R.
- [3] G. Häusler, "Verfahren und Vorrichtung zur Ermittlung der Form oder Abbildungseigenschaften von spiegelnden oder transparenten Objekten," DE19944354, 1999.

- [4] L. A. DeMars, A. H. Ramirez-Andrade, R. Porras-Aguilar, and K. Falaggis, "Super Sensitive Phase Measurement Deflectometry with effective fringe periods beyond the MTF limit," in *Optical Design and Fabrication 2019 (Freeform, OFT), OSA Technical Digest (Optical Society of America, 2019), paper OW4A.6*, 2019, p. 2.
- [5] M. C. Knauer, J. Kaminski, and G. Hausler, "Phase measuring deflectometry: a new approach to measure specular free-form surfaces," *Opt. Metrol. Prod. Eng.*, vol. 5457, no. September 2004, p. 366, 2004.
- [6] P. Su, Y. Wang, J. H. Burge, K. Kaznatcheev, and M. Idir, "Non-null full field X-ray mirror metrology using SCOTS: a reflection deflectometry approach," *Opt. Express*, vol. 20, no. 11, p. 12393, 2012.
- [7] Z. Zhang et al., "Full-field 3D shape measurement of specular surfaces by direct phase to depth relationship," Opt. Metrol. Insp. Ind. Appl. IV, vol. 10023, no. November 2016, p. 100230X, 2016.
- [8] Z. Niu, N. Gao, Z. Zhang, F. Gao, and X. Jiang, "3D shape measurement of discontinuous specular objects based on advanced PMD with bi-telecentric lens," Opt. Express, vol. 26, no. 2, p. 1615, 2018.
- [9] W. Li, M. Sandner, A. Gesierich, and J. Burke, "Absolute optical surface measurement with deflectometry," Interferom. XVI Appl., vol. 8494, no. September 2012, p. 84940G, 2012.
- [10] R. Huang, P. Su, J. H. Burge, and M. Idir, "X-ray mirror metrology using SCOTS/deflectometry," Adv. X-Ray/EUV Opt. Components VIII, vol. 8848, no. September 2013, p. 88480G, 2013.
- [11] G. Häusler, C. Richter, K.-H. Leitz, and M. C. Knauer, "Microdeflectometry—a novel tool to acquire three-dimensional microtopography with nanometer height resolution," *Opt. Lett.*, vol. 33, no. 4, p. 396, 2008.
- [12] C. Faber, E. Olesch, R. Krobot, and G. Häusler, "Deflectometry challenges interferometry: the competition gets tougher!," *Interferom. XVI Tech. Anal.*, vol. 8493, no. September 2012, p. 84930R, 2012.
- [13] S. Lowitzsch, J. Kaminski, M. C. Knauer, and G. Häusler, "Vision and modeling of specular surfaces," *Screen*, vol. 1, p. n1, 2005.
- [14] W. H. Southwell, "Wave-front estimation from wave-front slope measurements," *J. Opt. Soc. Am.*, vol. 70, no. 8, p. 998, 1980.
- [15] L. Huang, J. Xue, B. Gao, and C. Zuo, "Zonal wavefront reconstruction in quadrilateral geometry for phase measuring deflectometry," no. June, 2017.
- [16] H. Ren, F. Gao, and X. Jiang, "Least-squares method for data reconstruction from gradient data in deflectometry," *Appl. Opt.*, vol. 55, no. 22, p. 6052, 2016.
- [17] I. Mochi and K. A. Goldberg, "Modal wavefront reconstruction from its gradient," Appl. Opt., vol. 54, no. 12, p. 3780, 2015.
- [18] J. Ye *et al.*, "Modal wavefront estimation from its slopes by numerical orthogonal transformation method over general shaped aperture," *Opt. Express*, vol. 23, no. 20, p. 26208, 2015.
- [19] M. Aftab, J. H. Burge, G. A. Smith, L. Graves, C. jin Oh, and D. W. Kim, "Modal Data Processing for High Resolution Deflectometry," *Int. J. Precis. Eng. Manuf. Green Technol.*, vol. 6, no. 2, pp. 255–270, 2019.
- [20] E. Kewei, C. Zhang, M. Li, Z. Xiong, and D. Li, "Wavefront reconstruction algorithm based on Legendre polynomials for radial shearing interferometry over a square area and error analysis," *Opt. Express*, vol. 23, no. 16, p. 20267, 2015.
- [21] S. Ettl, E. Olesch, J. Kaminski, and H. S. G. Häusler, "Fast and robust 3D shape reconstruction from gradient data," *DGaO Proc.*, vol. 108, p. P 26, 2007.
- [22] L. Huang, M. Idir, C. Zuo, K. Kaznatcheev, L. Zhou, and A. Asundi, "Shape reconstruction from gradient data in an arbitrarily-shaped aperture by iterative discrete cosine transforms in Southwell configuration," *Opt. Lasers Eng.*, vol. 67, pp. 176–181, 2015.
- [23] L. Huang, J. Xue, B. Gao, C. McPherson, J. Beverage, and M. Idir, "Modal phase measuring deflectometry," *Opt. Express*, vol. 24, no. 21, p. 24649, 2016.
- [24] F. Zernike, "Difraction theory of the knife-edge test and its improved form, the phase-contrast method," *Mon. Not. R. Astron. Soc*, vol. 94, pp. 377–384, 1394.
- [25] G. W. Forbes, "Shape specification for axially symmetric optical surfaces," Opt. Express, vol. 15, no. 8, p. 5218, 2007.
- [26] G. W. Forbes and C. P. Brophy, "Asphere, O asphere, how shall we describe thee?," *Opt. Des. Eng. III*, vol. 7100, no. September 2008, p. 710002, 2008.
- [27] G. Forbes, "Better ways to specify aspheric shapes can facilitate design, fabrication, and testing alike," *Opt. InfoBase Conf. Pap.*, pp. 1–3, 2010.
- [28] G. W. Forbes, "Manufacturability estimates for optical aspheres," Opt. Express, vol. 19, no. 10, p. 9923, 2011.
- [29] G. W. Forbes, "Characterizing the shape of freeform optics," Opt. Express, vol. 20, no. 3, p. 2483, 2012.

[30] [31]	G. W. Forbes, "Fitting freeform shapes with orthogonal bases," <i>Opt. Express</i> , vol. 21, no. 16, p. 19061, 2013. G. Allaire and S. M. Kaber, <i>Numerical linear algebra</i> , vol. 55. Springer, 2008.